Breaking the adverse correlation between thermal stability and electrical insulation in polymer dielectrics by rearranging the donor and acceptor units

Jun-Wei Zha

zhajw@ustb.edu.cn

University of Science & Technology Beijing https://orcid.org/0000-0003-3301-3505

Yuting Wan

State Key Laboratory of Powder Metallurgy

Hang Luo

State Key Laboratory of Powder Metallurgy, Central South University

Zhongna Yan

School of Energy and Power Engineering, Changsha University of Science and Technology

Shuyi Shen

State Key Laboratory of Powder Metallurgy

Jiajun Peng

State Key Laboratory of Powder Metallurgy, Central South University

Xiaona Li

State Key Laboratory of Powder Metallurgy

Guanghu He

State Key Laboratory of Powder Metallurgy

Dou Zhang

State Key Laboratory of Powder Metallurgy, Central South University, Changsha, Hunan, China
https://orcid.org/0000-0001-8555-2784

Article

Keywords:

Posted Date: March 3rd, 2025

DOI: https://doi.org/10.21203/rs.3.rs-6051609/v1

Additional Declarations: There is **NO** Competing Interest.

Version of Record: A version of this preprint was published at Nature Communications on July 7th, 2025. See the published version at https://doi.org/10.1038/s41467-025-61539-x.

Abstract

Polymer dielectrics with enhanced thermal stability and electrical insulation are urgently needed for capacitive energy storage applications in electric power systems. There is a persistent challenge to break the contradictory correlation between high heat resistance and low electrical conduction in existing polymers. Here, we demonstrate a strategy for the effective rearrangement of short-range structural units within polyimide (PI) polymer chains through the preferred layer packing structure. This adaptable reorganization of monomeric units potently inhibits charge carrier transmission between the donor (diamine) and acceptor (dianhydride) moieties in PI chains, significantly reducing electrical conduction loss. The electrical conductivity of the designed polymer (named TPEI) is more than 3 orders of magnitude lower than that of commercial heat-resistant polymers. At the same time, this distinctive strategy is found to significantly improve the heat resistance of the modified polymer, with its glass transition temperature (T_g) rising from 236.31°C for pure PEI to 289.72°C for the TPEI. Consequently, ultrahigh discharged energy densities of 6.38 J cm^{-3} and 3.04 J cm^{-3}, with charge-discharge efficiencies above 90%, are achieved at 200 °C and 250 °C, respectively, demonstrating among the best in all-organic dielectric polymers. This work presents a feasible approach to break the adverse correlation between thermal stability and electrical insulation in PI materials.

Introduction

Dielectric capacitors, known for their characteristics of ultrafast charge-discharge speeds and high operating voltage, are prevalent in modern electronic devices and power systems[1, 2, 3]. Dielectric polymers have shown great potential in the field of electrostatic energy storage due to their high breakdown strength, light weight and facile processability[4, 5]. In recent decades, there was a growing demand for high-performance dielectrics that can operate stably under extreme conditions ranging from 150 °C to 250 °C, especially in the fields of clean energy, aerospace and oil/gas explorations[6, 7]. However, most polymers experience degraded electrical insulation at elevated operating temperatures. For instance, the charge-discharge efficiency of commercial biaxially oriented polypropylene (BOPP) remains at 95% at room temperature when the applied electric field is close to the breakdown limit, but sharply drops to below 65% at 120 °C[8].

Heat-resistant dielectric polymers with high glass transition temperatures (T_g) and melting points (T_m), such as polyimide (PI) and fluorene polyester (FPE), contain numerous highly conjugated structures that facilitate the movement of electrons, leading to a rapid increase in electrical conductivity under applied thermal and electric fields[9, 10, 11, 12, 13]. To suppress the migration of electrons in heat-resistant polymers, insulated inorganic fillers or molecular semiconductors are normally selected to be added into the host polymers to improve their high-temperature capacitive performance[14, 15, 16]. Additionally, cyclic-olefin polymers and fully alicyclic polymers with non-conjugated and non-planar structures have been synthesized and reported, aiming to increase their forbidden bandwidth (E_g) to achieve desirable electrical insulation[17, 18]. However, film dielectrics modified by these strategies show little improvement

in thermal stability, which results in a significant deterioration of capacitive performance for these polymers at operating temperatures between 200–250°C (higher than their T_g)[19, 20, 21].

In aromatic polyimides, intramolecular and intermolecular charge transfer complexes (CTC) can be easily formed between the donor (aromatic diamine) and acceptor (aromatic dianhydride) segments[22, 23]. Although the strong CTC effect gives rise to an increase in thermal stability, it significantly enhances the excitation and migration of electrons under elevated electric fields and high temperatures, ultimately leading to a sharp decrease in electrical insulation. Recently, a series of alicyclic polyimides has been reported to weaken the CTC effect of polymer chains [24, 25]. However, the synthetic process of the alicyclic polyimides is relatively complicated and immature, which hinders the application prospects of alicyclic polyimides in the market. Therefore, it is urgent to develop simple and commercially feasible methods to address the problem of increased electrical conduction loss in PI due to the CTC effect.

In this study, we first introduce a facile and practical strategy employing benzyl-induced crosslinking to interfere with the rearrangement of monomeric units within polymer chains. This approach leads to the formation of a preferred layer packing (PLP) structure in polymer dielectrics, thereby effectively mitigating the intermolecular CTC effect. The strategy simultaneously achieves suppressed high-temperature electrical conductivity and improved heat resistance in polymer dielectrics. Additionally, the experimental results demonstrate that the PLP structure is beneficial for the enhancement of the polymer modulus under high temperatures, thereby impeding the occurrence of electromechanical breakdown. Consequently, the resultant film exhibits an ultrahigh discharged energy density (U_e) of 6.38 J cm^{-3} at 200 ℃ and 3.04 J cm^{-3} at 250 ℃, with an η exceeding 90%. This work successfully demonstrates the feasibility of rearranging short-range structural units within polymer chains with outstanding capacitive energy storage performance in large-scale films under harsh environments.

Results and discussion

Structure design and characterization

A schematic of the two polymers, PEI and TPEI, synthesized from the commercial dianhydride monomer 4,4’-(4,4’-isopropylidenediphenoxy) diphthalic anhydride (BPADA) and the diamine monomers phenylenediamine (PDA) and 2,3,5,6-tetramethyl-1,4-phenylenediamine (TPD), is shown in Fig. 1a, with the fabrication process detailed in the experimental methods section. The chemical structure of prepolymers was confirmed by ^{1}HNMR (Figure S1, Supporting Information). These polymer films were obtained through thermal imidization within a temperature range of 70°C to 290°C in air, during which the polymer film containing benzyl functional groups underwent a thermo-oxidation crosslinking reaction. The crosslinking degree of the obtained TPEI film was measured using UV-vis spectroscopy (Figure S2, Supporting Information), and the result was 57.41%. Additionally, the quality of the polymer films was examined using atomic force microscopy (AFM) and scanning electron microscopy (SEM) (Figures S3-4, Supporting Information). The images reveal that polymer films are flat and free of apparent defects. As

shown in Fig. 1b, the adjacent stacking of electron-donating diamine moieties and electron-accepting dianhydride moieties in traditional aromatic polyimide chains, known as mixed layer packing (MLP) structure, facilitates the formation of intermolecular charge transfer complexes (CTC) effect. In contrast, the electron-donating diamine moieties and electron-accepting dianhydride moieties in polyimide chains are stacked individually, forming a structure known as preferred layer packing (PLP), which results in minimal intermolecular charge transfer effects (Fig. 1c). This unique benzyl-induced crosslinking aims to interfere with the rearrangement of electron-donating diamine and electron-accepting dianhydride units, creating the PLP structure in polymer dielectrics, which thereby enhance their thermal stability and capacitive energy storage performance.

To understand the formation of the PLP and MLP structure and their impacts on the electronic transitions in polymer film, we performed density functional theory (DFT) calculations to analyze the total energy variation and the electrostatic potential distribution among polymer chains. As shown in Fig. 2a**(i)**, in the PEI film, compare to the total energy of two molecular chains arranged in a PLP structure, the total energy of the two molecular chains arranged in a MLP structure reaches its lowest point at a distance of 5.1 Å. This indicates that the arrangement of PEI polymer chains primarily follows the MLP structure, which enhances electrostatic interactions among the polymer chains, resulting in a dramatic drop in energy storage performance. Conversely, there is no minimum total energy value for the arrangement of polymer chains in a PLP structure, indicating that the PLP structure is unstable. A benzyl-induced crosslinking method is utilized to create the PLP structure within polymer chains, significantly diminishing electrostatic interactions among them (Fig. 2c-d**(i)**). Additionally, the local interchain spacing in the polymer chains is increased by leveraging the electrostatic repulsion at the same positions between molecular chains, leading to difficulty in the transport of charge carriers within the polymer. Furthermore, the interfragment CT (IFCT) method in Multiwfn[26] revealed that 0.92 electrons are transferred from the donor (diamine) to acceptor (dianhydride) during charge-transfer (CT) excitation of PEI (Fig. 2b**(ii)**). Notably, in the PLP structure induced by benzyl-induced crosslinking, the transfer of electrons from the diamine to the dianhydride during CT excitation is significantly diminished, with the amount of charge transfer nearly approaching 0 electrons between the two cross-linked molecular chains (Fig. 2c-d**(ii)**). This strongly supports the idea that PLP structure effectively restricts electronic transport between polymer dielectrics. Furthermore, the substituents on the benzene rings can influence the twisting of the molecular chain conformation, thereby diminishing the electrostatic interactions within the molecular chains [10](Figure S5, Supporting Information).

The chemical structure of PEI and TPEI films was analyzed using FT-IR spectroscopy, as shown in Fig. 3a. The characteristic peaks observed at wavenumbers of 1780 cm^{-1}, 1720 cm^{-1}, 1350 cm^{-1}, and 740 cm^{-1} are attributed to the vibrational modes associated with the imide rings. Additionally, the absorption bands at 1850 cm^{-1} and 1110 cm^{-1} correspond to the vibrations of -CO-O-CO- and aliphatic -C-O-C- groups, respectively, indicating the presence of benzyl-induced crosslinked structure. Moreover, the results of X-ray photoelectron spectroscopy (XPS) for TPEI and uncross-linked TPEI ($TPEI_u$) films also demonstrate the formation of aliphatic -C-O-C- groups at the crosslinked positions (Figure S6,

Supporting Information). The signals at 533.3 eV in the O1s spectrum and 286.6 eV in the C1s spectrum are assigned to the -C-O-C- groups, with a greater percentage observed in TPEI compared with $TPEI_u$. The critical role of oxygen (O_2) in the thermal-oxidative degradation and benzyl-induced crosslinking of polymers containing benzyl groups is confirmed by TGA (Fig. 3b)[27, 28, 29]. Compared with the TGA curve of the $TPEI_u$ measured in an inert atmosphere (N_2), the TGA curve of the $TPEI_u$ tested in air shows a significant increase in residual weight within a temperature range of 280 ℃ to 380 ℃. This phenomenon further indicates the correlation of the thermos-oxidative crosslinking reaction with O_2 and benzyl groups.

The glass transition temperature (T_g) increases from 236.31 ℃ for PEI to 289.72 ℃ for TPEI, suggesting that the movement of polymer chains is restrained by benzyl-induced crosslinking networks (Fig. 3c). In addition, the variation in specific heat capacity (ΔC_p) during the glass transition, caused by changes in the conformation of polymer chains, was obtained from DSC data. ΔC_p is significantly reduced from 0.205 J g^{-1} °C^{-1} for PEI to 0.119 J g^{-1} °C^{-1} for TPEI, indicating that the polymer chains in the crosslinked films are both stretched and tightly stacked, thereby minimizing voids and defects in the polymer films[16, 30]. Moreover, the results of the in-plane thermal dimension change curves show a lower coefficient of thermal expansion (CTE) in TPEI films compared to that of in PEI films in a specific temperature range (Fig. 3d). These results indicate that benzyl-induced crosslinking network effectively restricts movement of polymer chains, thereby improving the thermal stability of the polymer films. As shown in Figs. 3e-f, the exploded views of the XRD patterns of the films indicate the presence of “ch-pack” ordered domains observed in TPEI compared with PEI[31]. The “ch-pack” packing structure of polymer chains, similar to the PLP structure, originates from liquid-crystalline-like ordered domains. Hence, the PLP structure formed by benzyl-induced crosslinking predominates in TPEI film, indicating an efficient reduction in electrical conduction loss. In contrast, the main ordered packing structure in PEI is a “π-stack” formation, which represents the π-π stacking of imide and phenyl rings in ordered domains, thereby largely promoting charge carrier transport in polymers. Notably, the variation in interchain spacing of polymer chains was calculated from the XRD data of PEI and TPEI films, which is consistent with the theoretical charge results from DFT calculations. (Figure S7, Supporting Information)

Mechanical strengthening and electrical insulation mechanisms

The high-field electrical insulation properties of polymeric materials at elevated temperatures are closely linked to the electromechanical breakdown process. Under an external electric field (*E*), the thickness of polymer films decreases due to the increasing electrostatic stress ($= \frac{1}{2}\epsilon_0\epsilon_r E^2$, where ϵ_0 and ϵ_r denote the dielectric permittivity of a vacuum and the dielectric constant of dielectrics, respectively), which is counterbalanced by the mechanical stress arising from elastic deformation ($= Ye$, where Y is the modulus and e represents the elastic strain of the dielectric). The increased breakdown strength of the polymer films can be attributed to their greater modulus. The storage modulus of TPEI (for example, 4.46 GPa at 150 ℃, 3.97 GPa at 200 ℃ and 3.42 GPa at 250 ℃) is greater than that of PEI (for example,

2.82 GPa at 150 ℃, 2.46 GPa at 200 ℃ and 0 GPa at 250 ℃), throughout a temperature range of 35 ℃ to 250 ℃ (Figs. 4a-c).

Another advantage of the TPEI film is its excellent electrical insulation performance at high temperatures. According to the tested results of leakage current density of the polymer films (Figs. 4d-e and Figure S8 in the Supporting Information), TPEI exhibits over an order of magnitude lower leakage current density than that of PEI and other heat-resistant polymers at high electric fields and elevated temperatures. For instance, at 200°C and 300 MV m^{-1}, the leakage current density decreases from 1.19 × 10^{-5} A cm^{-2} for PEI to 4.46 × 10^{-7} A cm^{-2} for TPEI, indicating that the PLP structure in TPEI polymer can significantly suppress the conduction loss from the injected and excited charge carriers under extreme conditions. Simultaneously, the hopping distance (λ, derived from the hopping conduction model, detailed in the Supporting Information) decreases from 1.983 nm for PEI films to 1.17 nm for TPEI, indicating a higher charge trap density and a deeper charge trap depth in the TPEI film. Notably, at 250°C, the leakage current density of TPEI is 2.35 × 10^{-6} A cm^{-2} at 300 MV m^{-1} (Figure S8, Supporting Information), which is significantly lower than that of existing heat-resistant polymers. Additionally, TPEI exhibits the lowest electrical conductivity over a temperature range from 50°C to 250°C (Fig. 4f), which is several orders of magnitude lower than that of other heat-resistant polymers, including PEI, FPE, Kapton, and copolymer of PEI with polysulfone (PEI-PSU). For instance, the electrical conductivity of TPEI is 4.66 × 10^{-13} S m^{-1}, whereas the value of the PEI-PSU is 5.07× 10^{-9} S m^{-1} at 250°C.

Dielectric properties and capacitive energy storage performance

According to the equation ($U_e = \frac{1}{2}\epsilon_0\epsilon_r E_b^2$, where E_b denotes the breakdown strength of dielectrics), a high dielectric constant (ϵ_r) and a high intrinsic E_b are crucial for achieving outstanding discharged energy density (U_e) in a linear dielectric. The dielectric constant (ϵ_r) and dielectric loss (tan δ) of PEI and TPEI were tested as functions of frequencies and temperatures (see Fig. 5a-b). A higher ϵ_r of 3.85 is observed for TPEI, compared with 3.43 for PEI, at 1 kHz and room temperature. The enhancement of ϵ_r in TPEI is likely due to the formation of flexible aliphatic ether linkages (-C-O-C-) among adjacent polymer chains through benzyl-induced crosslinking. This acts as “lubricating agents” to weaken dipole-dipole interactions, thereby improving the dipole polarization capability. Moreover, when the temperatures close to the T_g of PEI, the local motions of the polymer chains become more pronounced, leading to a significant increase in ϵ_r and tan δ. In contrast, the dielectric properties of TPEI are highly stable within a wide temperature range from 30°C to 250°C.

Next, the breakdown strength (E_b) and the shape parameter (β) of PEI and TPEIat high temperatures were estimated using a two-parameter Weibull statistic method (details are shown in the Supporting Information). A higher value of β indicates better stability of the polymer dielectric. As shown in Figs. 5c-d, the breakdown strength (E_b) of TPEI is 734.27 MV m^{-1} at 150°C and 661.87 MV m^{-1} at 200°C, both of which surpass the reported values of most heat-resistant polymers. For instance, at 150°C, the E_b of PEI

are 513.22 MV m^{-1}, while that of polytetrafluoroethylene (PTFE) is 396 MV m^{-1}. At 200°C, the values are 428.84 MV m^{-1} for PEI and 368 MV m^{-1} for PTFE. Notably, TPEI exhibits an ultrahigh E_b of 570.8 MV m^{-1} at 250°C (Figs. 5e-f), surpassing that of existing dielectric polymers under the same conditions. For instance, the breakdown strength (E_b) of Al-1 PI and c-BCB are 541 MV m^{-1} and 262 MV m^{-1}, respectively, at 250°C[9, 25]. Furthermore, a notable increase of the β is observed in TPEI, for example, with a value of 24.1 for TPEI compared with 10.98 for PEI at 200°C. This suggests that TPEI shows improved dielectric reliability at elevated temperatures. These improvements can be attributed to the significantly enhanced storage modulus and reduced electrical conductivity resulting from the PLP structure formed by benzyl-induced crosslinking in the polymers.

The capacitive energy storage performance of benzyl-induced crosslinking polymers, with varying quantity of benzyl, and PEI was tested at 150°C and 200°C (Figures S9-12, Supporting Information). It has been found that TPEI (with diamine monomers containing 4 benzyl groups) exhibits the best capacitive performance, for example, a discharged energy density (U_e) of 8.85 J cm^{-3} at 760 MV m^{-1} and 150°C, as well as a U_e of 7.16 J cm^{-3} at 660 MV m^{-1} and 200°C (Figs. 6a-b). Notably, Figs. 6a-d and S13-16 demonstrate that TPEI exhibits significant advantages compared with state-of-the-art commercial heat-resistant polymers such as PEI, Kapton, FPE, and PEI-PSU. Additionally, at $\eta \geq 90\%$, TPEI exhibits an ultrahigh U_e of 6.38 J cm^{-3} at 200°C and 3.04 J cm^{-3} at 250°C, surpassing that of most reported works (Figs. 6e-f). Moreover, TPEI can continuously undergo charge-discharge cycling for 100,000 cycles at 200°C and 200 MV m^{-1} (Figure S17a, Supporting Information), indicating that it possesses outstanding long-term stability in energy storage performance at high temperatures. Next, the fast discharge capability of TPEI at 200 ℃ and BOPP at 120°C were measured (Figure S17b, Supporting Information). The results show that the discharge time (τ_{95}, defined as the time needed to discharge 95% of the charged energy density) for TPEI is equivalent to that of BOPP at 120°C. However, the power density of TPEI (0.16 MW cm^{-3} at 200°C) is higher than that of BOPP (0.10 MW cm^{-3} at 120°C) under the same electric field, suggesting a significantly enhanced discharge capability of TPEI films.

Conclusion

This work offers an effective strategy for the synthesis of heat-resistant insulative dielectric polymers. The unique preferred layer packing (PLP) structure, formed by benzyl-induced crosslinking methods within intricately arranged polymer chains, significantly enhances the thermal stability and electrical insulation of polymer dielectrics. The lowest electrical conductivity of the designed homopolymer, in comparison with existing polymeric materials, is achieved at elevated temperatures. Therefore, an ultrahigh discharged energy density ($\eta > 90\%$) of 6.38 J cm^{-3} (200°C) and 3.04 J cm^{-3} (250°C) are achieved in TPEI, which is higher than that of most reported works. This study presents a simple method for large-scale production of dielectric films to address the challenge of insufficient capacitive energy storage performance under extreme conditions in heat-resistant polymer dielectrics.

Experimental Methods

Materials

4,4’-(4,4’-isopropylidenediphenoxy) diphthalic anhydride (BPADA), 1,4-phenylenediamine (PDA), 2,5-diaminotoluene (DNT), 2,5-dimethyl-1,4-phenylenediamine (DPD), 2,3,5,6-tetramethyl-1,4-phenylenediamine (TPD) were purchased from Tokyo Chemical Industry. The pyromellitic dianhydride (PMDA) and 4,4’-oxydianiline (ODA) were purchased from Shanghai Aladdin Biochemical Technology Co., Ltd. Copolymer of PEI with polysulfone (PEI-PSU) particles (T_g ≈ 265°C), fluorene polyester (FPE) particles (T_g = 330°C) and commercial biaxially oriented polypropylene (BOPP) films with the thickness of 5.8 μm were provided by Polyk Technologies Company. N-methyl-2-pyrrolidinone (NMP) was obtained from Sinopharm Chemical Reagent Co., Ltd. All materials were used as received without further purification.

Synthesis of polymer films

A certain molarity of diamine monomer was dissolved into the NMP solution. Then, the same molar amount of dianhydride monomer was added into the mixed solution, and stirred at room temperature for 36h to synthesize a viscous poly(amic acid) solution. The reaction solution was drop-cast on a clean glass slide and baked in a circulation oven at 85 ℃ for 2h, 110 ℃ for 1h, 160 ℃ for 1h, and 220 ℃ for 1h to remove the substantial solvent and form imide rings. Then, the glass slide was kept at 260 ℃ for 1h, and then at 290 ℃ for 1.5h to induce benzyl crosslinking and remove the residual solvent. The polymer films were peeled off from the glass slides in deionized water and dried in a vacuum oven at 110 ℃ for 24h to remove the residual moisture. The polymer films named PEI, 1CH_3-PEI, 2CH_3-PEI, amd TPEI are synthesized from BPADA and PDA, DNT, DPD, and TPD, respectively, following the preparation process outlined above. In addition, the uncross-linked TPEI (labeled $TPEI_u$) was synthesized using a similar preparation method, with the exception of the heat treatment conditions, where a vacuum oven was employed. Kapton film, which has the same structure as commercial Kapton polyimide, is obtained through a reaction between PDMA and ODA. The curing reaction of Kapton films proceeded according to the following process: 80 ℃/3h, 100 ℃/1h, 150 ℃/1h, 200 /1h, 250 ℃/1h, 300 ℃/1h, and 350 ℃/2h. PEI-PSU and FPE polymer films were prepared as comparison samples using the solution casting method. PEI-PSU particles and FPE particles were dissolved in NMP stirring at 70°C for 24 h. Next, the viscous polymer solution was cast and baked at 70°C for 2 h, and then the sample films were dried in a vacuum oven at 200°C for 24 h.

Characterization

^{1}H nuclear magnetic resonance (NMR) spectra of the prepolymers were recorded using a JNM-ECZ600R spectrometer in DMSO-d_6. The crosslinking degree of the films was determined by calculating the

absorbance of the polymer solutions, which was recorded using a UV-vis spectrophotometer (UV-2600i, Island Ferry, Japan). The morphologies of the polymer films were observed by a scanning electron microscope (SEM, TESCAN) and an atomic force microscope (NanomanTM VS, USA). X-ray photoelectron spectroscopy (XPS) analysis was carried out by a Thermo Fisher K-Alpha spectroscopy with an Al source. Fourier transform infrared (FTIR) spectra of the samples were used to confirm their characteristic functional groups by a Nicolet iS50 FTIR spectrometer. X-ray diffraction (XRD) analysis was conducted with Cu radiation by a PANalytical Empyren diffractometer. Thermogravimetric analysis (TGA) curves were obtained from a NETZSCH TGA209F1 thermogravimetry under nitrogen (air) atmosphere at a heating rate of 10°C min^{-1} ranging from 30°C to 800°C. Differential scanning calorimetry (DSC) was performed on a TA Q10 DSC at a scan rate of 10°C min^{-1} ranging from 30°C to 300°C in a nitrogen atmosphere. The in-plane thermal expansion change curves of the films were recorded by a TMA Q400 from TA Instruments, with a force of 0.02 N, under nitrogen flow at a heating rate of 5°C min^{-1} ranging from 30°C to 350°C. Dynamic mechanical analysis (DMA) of the samples was conducted using a DMA 850 TA Instruments at a heating rate of 5°C/min and a load frequency of 1 Hz under nitrogen flow. Au electrodes with diameters of 3 mm and 8 mm were coated onto both sides of the films using a GVC-2000 magnetron ion sputtering instrument for electrical testing under high electric field (D-E loop, breakdown strength and leakage current) and low electric field (dielectric spectra), respectively. The dielectric frequency spectrum and dielectric temperature spectrum of the samples were measured using a precision impedance analyzer (Agilent 4294A, Germany) and a DMS-500 dielectric temperature spectroscopy measurement system (DMS-500, China), respectively. The high-temperature-resistivity of the films was tested using a Tonghui TH2690A insulation resistance meter. The displacement-electric field hysteresis loop (D-E loop), breakdown strength, leakage current, and cyclic charge-discharge performance of the samples were measured by a TF Analyzer 3000 series (AixACT, Germany) at 100 Hz. The fast charge-discharge tests were proceeded using a DCQ-20A measurement system (Polyk Technologies) with a load resistor (RL) of 10 kΩ.

DFT calculations

The ground-state geometry optimizations and energy scanning of the polymer structural units were performed by the Gaussian 16 with the B3LYP hybrid function and 6-31G (d) basis function. The structure construction and the visualization of electrostatic potential distribution of polymer units was conducted by GaussView 6.1 and Multiwfn 3.8. [44, 45, 46] The model construction of polymer structural units for energy scanning was completed by dimerscan and xyz2QC. [47]

Declarations

Acknowledgments This work was supported by the National Natural Science Foundation of China (52172265), Excellent Youth Science Foundation of Hunan Province (2022JJ20067), The Science and Technology Innovation Program of Hunan Province (2022RC1074), Central South University Innovation-

Driven Research Program (2023CXQD010), and the State Key Laboratory of Powder Metallurgy, Central South University, Changsha, China.

Author Contributions Y.W. and H.L conceived the idea and designed the research. Y.W. carried out experiments, analyzed the data. Y.W., H.L., Z.Y., S.S., J.P., X.L., G.H., J.Z. and D.Z. analyzed the data and participated in helpful discussions. Y.W., H.L., D.Z. and J.Z. wrote the first draft of the manuscript, with input from all authors.

Competing interests All authors declare no competing interests.

References

1. Sarjeant WJ, Clelland IW, Price RA. Capacitive components for power electronics. *Proc IEEE* **89**, 846-855 (2001).
2. Yang L*, et al.* Perovskite lead-free dielectrics for energy storage applications. *Prog Mater Sci* **102**, 72-108 (2019).
3. Zhang M*, et al.* Ultrahigh energy storage in high-entropy ceramic capacitors with polymorphic relaxor phase. *Science* **384**, 185-189 (2024).
4. Chu B*, et al.* A dielectric polymer with high electric energy density and fast discharge speed. *Science* **313**, 334-336 (2006).
5. Luo H*, et al.* Progress on polymer dielectrics for electrostatic capacitors application. *Adv Sci* **9**, (2022).
6. Watson J, Castro G. High-temperature electronics pose design and reliability challenges. *Analog Dialogue* **46**, 3-9 (2012).
7. Li Q, Yao F-Z, Liu Y, Zhang G, Wang H, Wang Q. High-temperature dielectric materials for electrical energy storage. *Annu Rev Mater Res* **48**, 219-243 (2018).
8. Zhou Y*, et al.* A scalable, high-throughput, and environmentally benign approach to polymer dielectrics exhibiting significantly improved capacitive performance at high temperatures. *Adv Mater* **30**, (2018).
9. Li Q*, et al.* Flexible high-temperature dielectric materials from polymer nanocomposites. *Nature* **523**, 576-579 (2015).
10. Wang R*, et al.* Designing tailored combinations of structural units in polymer dielectrics for high-temperature capacitive energy storage. *Nat Commun* **14**, (2023).
11. Dong J*, et al.* Scalable polyimide-organosilicate hybrid films for high-temperature capacitive energy storage. *Adv Mater* **35**, (2023).
12. Yan C*, et al.* Improved capacitive energy storage at high temperature via constructing physical cross-link and electron–hole pairs based on p-type semiconductive polymer filler. *Adv Funct Mater* **34**, (2023).

13. Yang M*, et al.* Surface ion-activated polymer composite dielectrics for superior high-temperature capacitive energy storage. *Energy Environ Sci* **17**, 1592-1602 (2024).
14. Yuan C*, et al.* Polymer/molecular semiconductor all-organic composites for high-temperature dielectric energy storage. *Nat Commun* **11**, (2020).
15. Dai Z*, et al.* Scalable Polyimide-Poly(Amic Acid) Copolymer Based Nanocomposites for High-Temperature Capacitive Energy Storage. *Adv Mater* **34**, (2021).
16. Yang M*, et al.* Roll-to-roll fabricated polymer composites filled with subnanosheets exhibiting high energy density and cyclic stability at 200 °C. *Nat Energy* **9**, 143-153 (2024).
17. Deshmukh AA*, et al.* Flexible polyolefin dielectric by strategic design of organic modules for harsh condition electrification. *Energy Environ Sci* **15**, 1307-1314 (2022).
18. Chen J*, et al.* Ladderphane copolymers for high-temperature capacitive energy storage. *Nature* **615**, 62-66 (2023).
19. Wu C, Deshmukh AA, Chen L, Ramprasad R, Sotzing GA, Cao Y. Rational design of all-organic flexible high-temperature polymer dielectrics. *Matter* **5**, 2615-2623 (2022).
20. Chen J*, et al.* Aromatic-free polymers based all-organic dielectrics with breakdown self-healing for high-temperature capacitive energy storage. *Adv Mater* **35**, (2023).
21. Pei Z*, et al.* Wide bandgap heterostructured dielectric polymers by rapid photo-crosslinking for high-temperature capacitive energy storage. *Adv Funct Mater* **34**, (2023).
22. Hasegawa M, Horie K. Photophysics, hotochemistry, and optical properties of polyimides. *Prog Polym Sci* **26**, 259-335 (2001).
23. Zhuang Y, Seong JG, Lee YM. Polyimides containing aliphatic/alicyclic segments in the main chains. *Prog Polym Sci* **92**, 35-88 (2019).
24. Song J*, et al.* Alicyclic polyimides with large band gaps exhibit superior high-temperature capacitive energy storage. *Mater Horiz* **10**, 2139-2148 (2023).
25. Ren W*, et al.* Metallized stacked polymer film capacitors for high-temperature capacitive energy storage. *Energy Storage Mater* **65**, (2024).
26. Lu T, Chen F. Multiwfn: A multifunctional wavefunction analyzer. *J Comput Chem* **33**, 580-592 (2011).
27. Song Q*, et al.* Controlled thermal oxidative crosslinking of polymers of intrinsic microporosity towards tunable molecular sieve membranes. *Nat Commun* **5**, (2014).
28. Zhu S*, et al.* Benzyl-induced crosslinking of polymer membranes for highly selective CO2/CH4 separation with enhanced stability. *Macromolecules* **55**, 6890-6900 (2022).
29. Wang F, Zhao G, Liu Y, Tang G, Qin P, Li P. Development of phenolphthalein-based copolyimides and their derivative cross-linked and thermally rearranged polymers for gas separation. *Macromolecules* **57**, 1370-1382 (2024).
30. Yang M, Zhou L, Li X, Ren W, Shen Y. Polyimides physically crosslinked by aromatic molecules exhibit ultrahigh energy density at 200 °C. *Adv Mater* **35**, (2023).

31. Wakita J, Jin S, Shin TJ, Ree M, Ando S. Analysis of molecular aggregation structures of fully aromatic and semialiphatic polyimide films with synchrotron grazing incidence wide-angle X-ray scattering. *Macromolecules* **43**, 1930-1941 (2010).
32. Dong J*, et al.* Scalable high-permittivity polyimide copolymer with ultrahigh high-temperature capacitive performance enabled by molecular engineering. *Adv Energy Mater* **14**, (2023).
33. Yang M*, et al.* Quantum size effect to induce colossal high-temperature energy storage density and efficiency in polymer/inorganic cluster composites. *Adv Mater* **35**, (2023).
34. Zhang B*, et al.* Superior High-Temperature Energy Density in Molecular Semiconductor/Polymer All-Organic Composites. *Adv Funct Mater* **33**, (2022).
35. Yang M*, et al.* Sub-Nanowires Boost Superior Capacitive Energy Storage Performance of Polymer Composites at High Temperatures. *Adv Funct Mater* **33**, (2023).
36. Zhou Y, Zhu Y, Xu W, Wang Q. Molecular Trap Engineering Enables Superior High-Temperature Capacitive Energy Storage Performance in All-Organic Composite at 200 °C. *Adv Energy Mater* **13**, (2023).
37. Yang M, Wang Z, Zhao Y, Liu Z, Pang H, Dang ZM. Unifying and suppressing conduction losses of polymer dielectrics for superior high-temperature capacitive energy storage. *Adv Mater*, (2023).
38. Liu M*, et al.* Significant enhancement in dielectric properties of polyimide alloys through a two-phase interlocking structure. *Adv Funct Mater* **34**, (2024).
39. Ran Z*, et al.* Spiral-structured dielectric polymers exhibiting ultrahigh energy density and charge–discharge efficiency at high temperatures. *Adv Mater* **35**, (2023).
40. Shukla S*, et al.* Pendant group functionalization of cyclic olefin for high temperature and high-density energy storage. *Adv Mater*, (2024).
41. Pei JY*, et al.* Flexible high-temperature polymer dielectrics induced by ultraviolet radiation for high efficient energy storage. *Adv Funct Mater*, (2024).
42. Tian Y*, et al.* Intrinsic-designed polyimide dielectric materials with large energy storage density and discharge efficiency at harsh ultra-high temperatures. *Mater Horiz* **10**, 5835-5846 (2023).
43. Wang Y*, et al.* Sandwiched polymer nanocomposites reinforced by two-dimensional interface nanocoating for ultrahigh energy storage performance at elevated temperatures. *Small* **19**, (2023).
44. Manzetti S, Lu T. The geometry and electronic structure of Aristolochic acid: possible implications for a frozen resonance. *J Phys Org Chem* **26**, 473-483 (2013).
45. Lu T, Manzetti S. Wavefunction and reactivity study of benzo[a]pyrene diol epoxide and its enantiomeric forms. *Struct Chem* **25**, 1521-1533 (2014).
46. Zhang J, Lu T. Efficient evaluation of electrostatic potential with computerized optimized code. *Physical Chemistry Chemical Physics* **23**, 20323-20328 (2021).
47. Lu T.). Molclus program, Version 1.12.

Figures

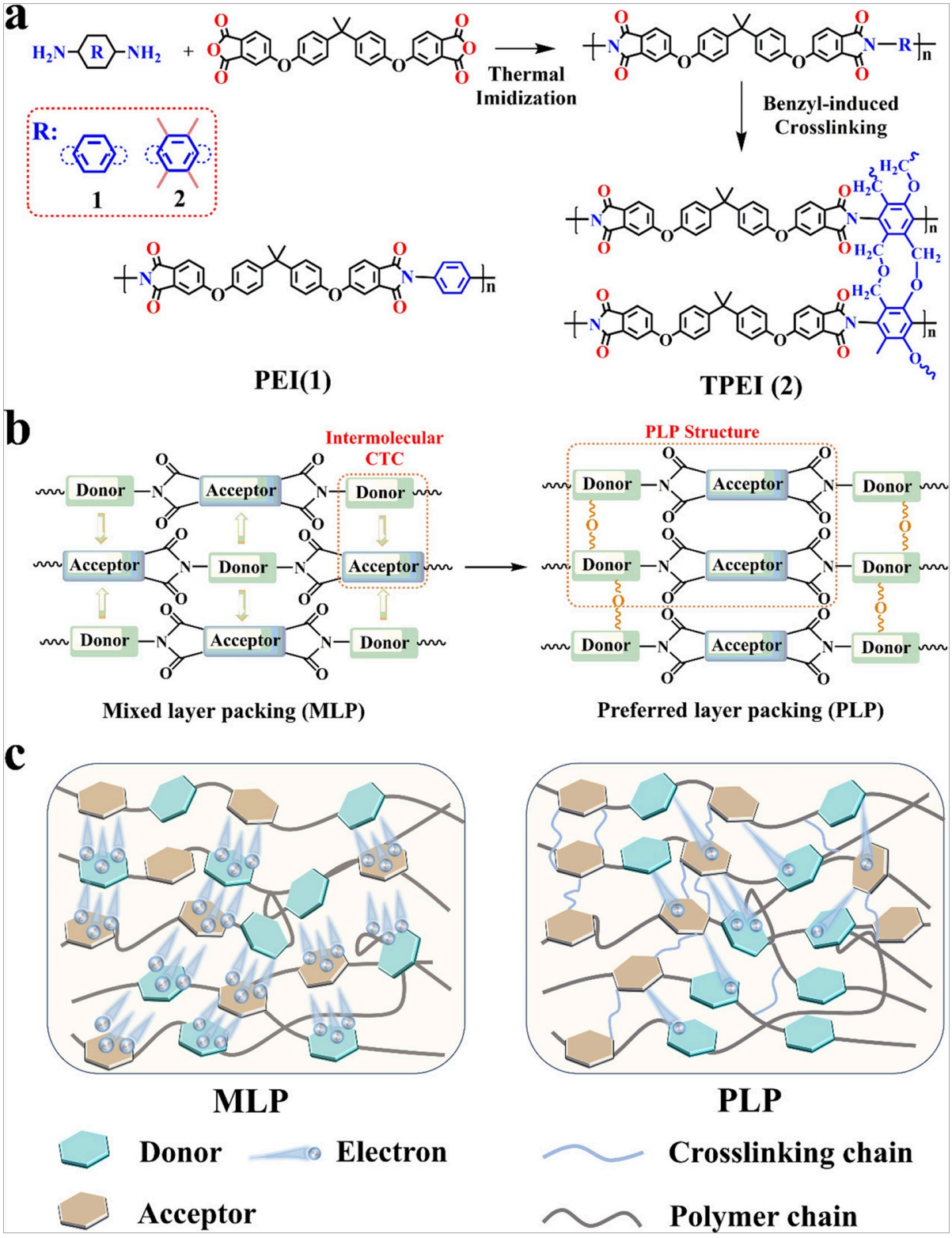

Figure 1

Schematic illustration of the construction of the PLP structure in dielectric polymers. a) Synthetic chemical structures of PEI and TPEI with benzyl-induced crosslinking. b) A detailed schematic design of the PLP structure transformed from the MLP structure. c) Schematic of electron transport within MLP and PLP structure.

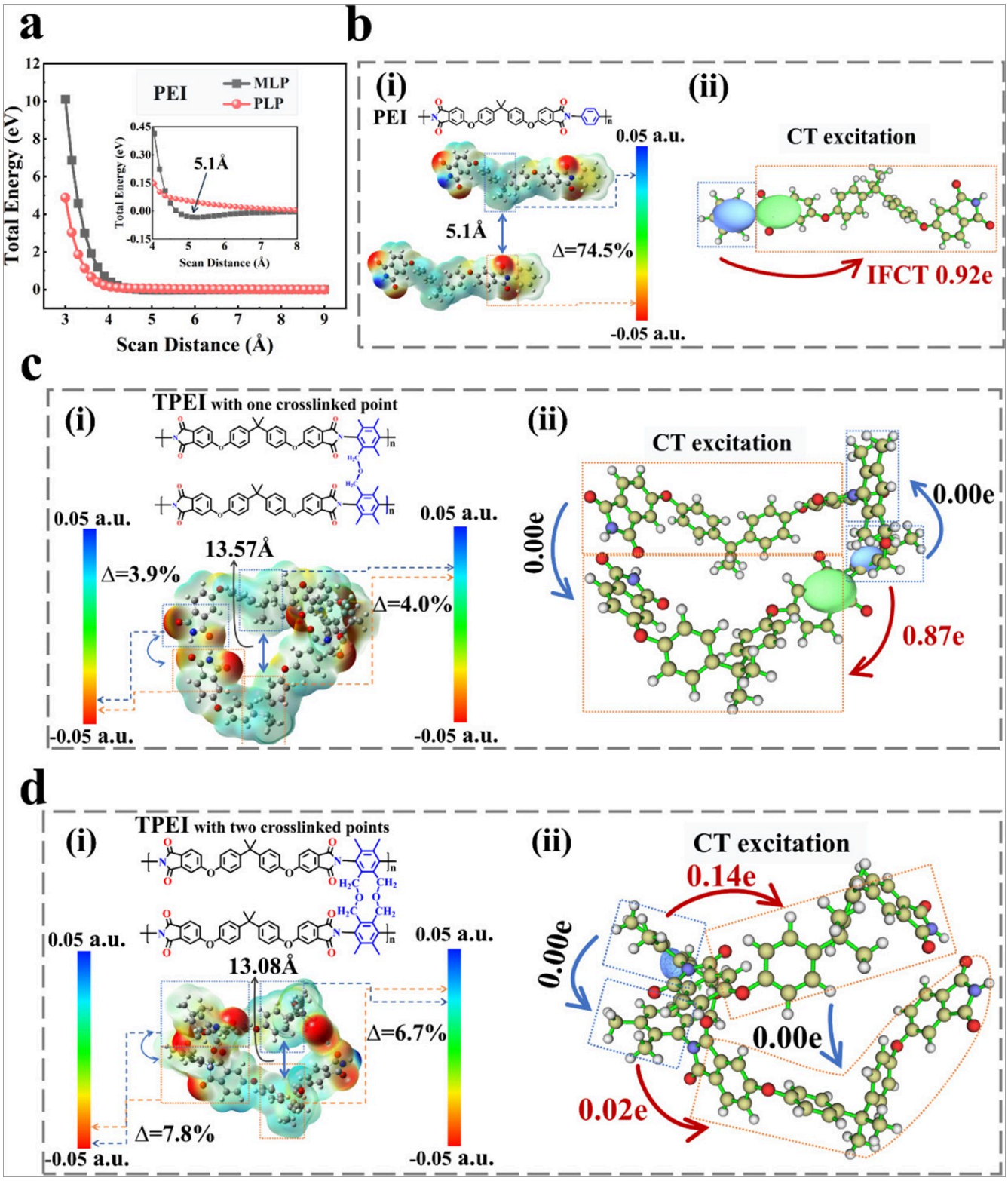

Figure 2

The feasibility of the PLP structure in the field of polymer energy storage verified by theoretical calculation. a) The total energy of the MLP and PLP of the PEI molecular chain as a function of scan distance (Inset: partial enlarged detail of energy scanning). (i) Schematic chemical structures and electrostatic potential distributions and (ii) using the interfragment CT (IFCT) method to evaluate amount of electron transfer between the donor (diamine) and acceptor (dianhydride)during charge-transfer (CT)

excitation and Chole-Cele distribution map of b) PEI, c) TPEI with one crosslink point and d) TPEI with two crosslink points. The marks of color bars indicate the difference in electrostatic potential between the two polymer chains.

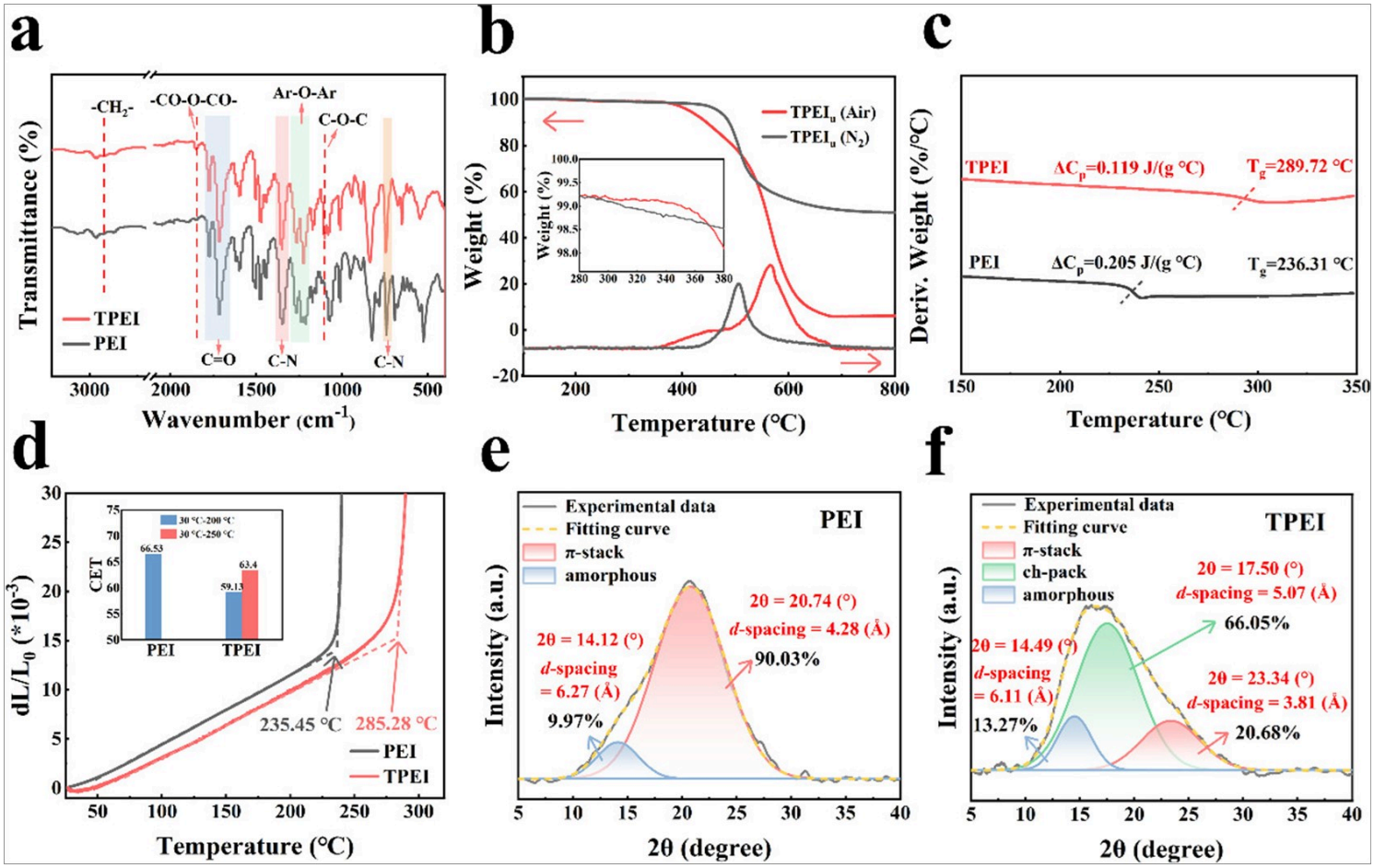

Figure 3

Characterization of the polymer films and the PLP structure. a) FT-IR spectra, b) TGA and DTG curves (Inset: partial enlarged detail of TGA), c) DSC curves, d) In-plane thermal expansion change curves (Inset: CET values) for PEI and TPEI films. Exploded view of the XRD pattern for e) PEI film and f) TPEI film.

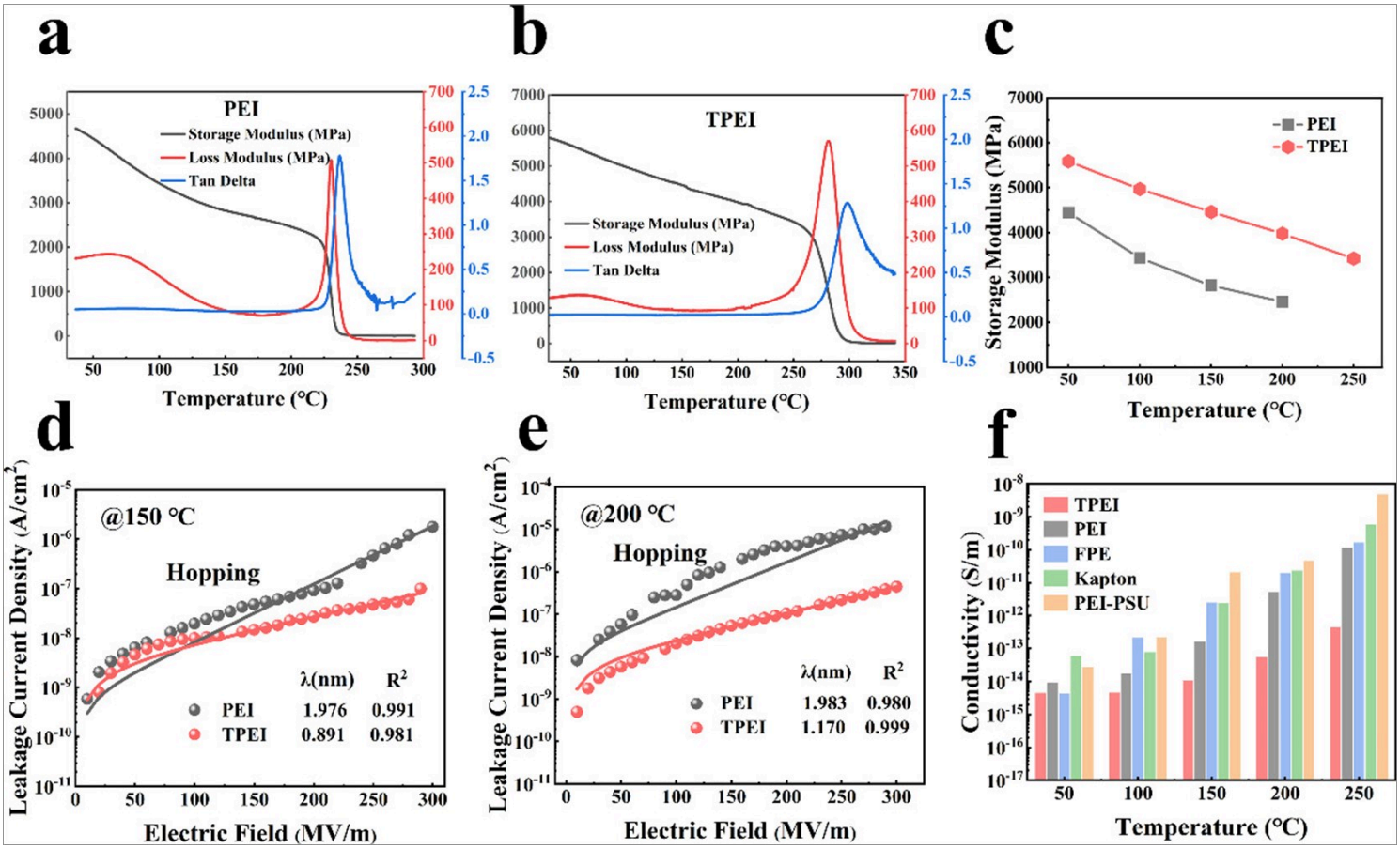

Figure 4

Analysis of mechanical performance and electrical insulation properties. DMA curves for a) PEI film and b) TPEI film. c) Comparison of the storage modulus of PEI and TPEI films. d) Leakage current density of polymer films as a function of electric field at 150 °C and e) 200 °C. f) Electrical conductivity of TPEI, PEI, FPE, Kapton, and PEI-PSU films at various temperatures.

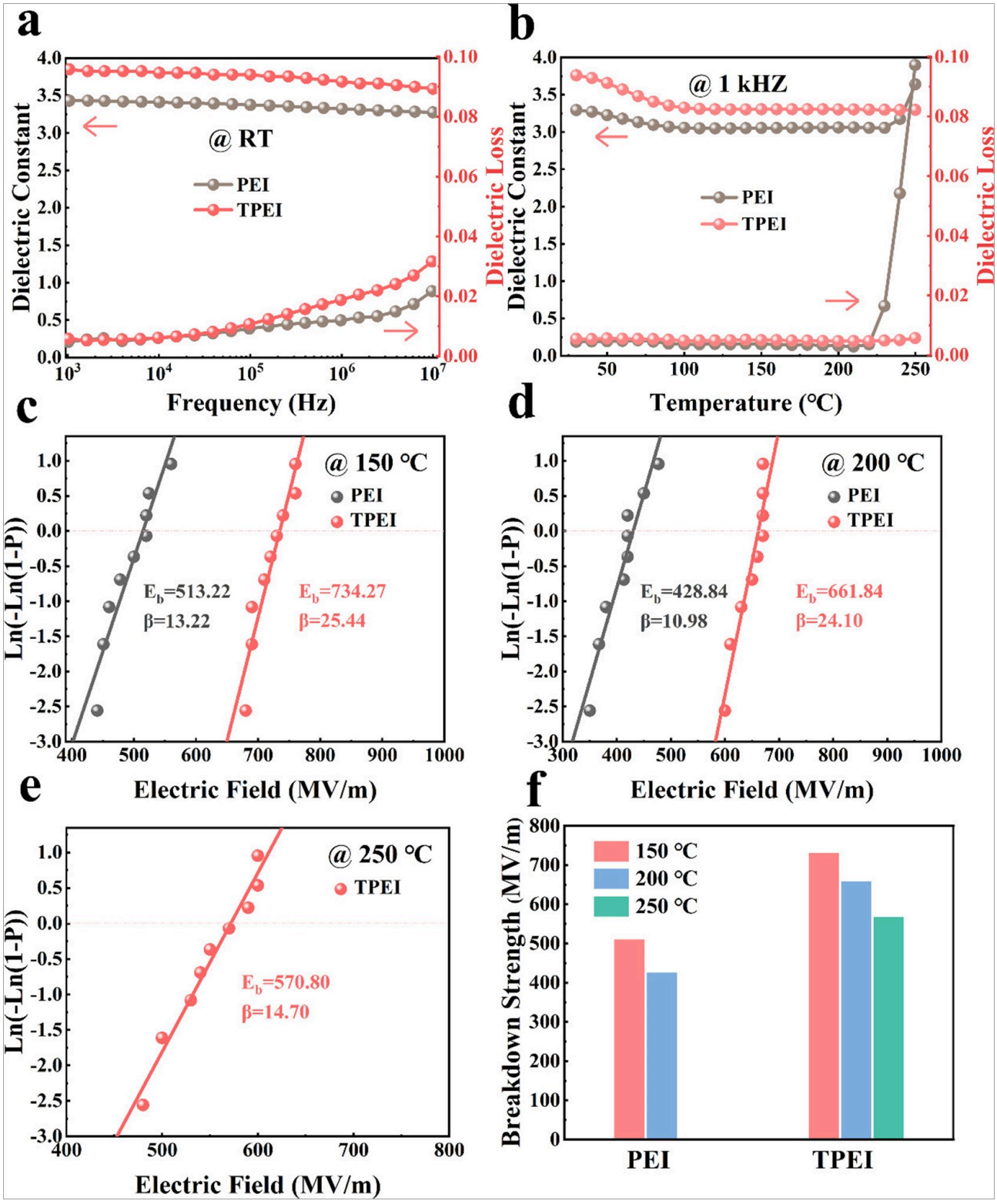

Figure 5

Dielectric properties and electrical breakdown performance. a) Dielectric frequency spectrum and b) dielectric temperature spectrum of PEI and TPEI films. Weibull distribution of the characteristic breakdown strength of PEI and TPEI polymers at c) 150 °C and d) 200 °C. e) Weibull distribution of characteristic breakdown strength for TPEI samples at 250 °C. d) breakdown strength of PEI and TPEI films at different temperatures.

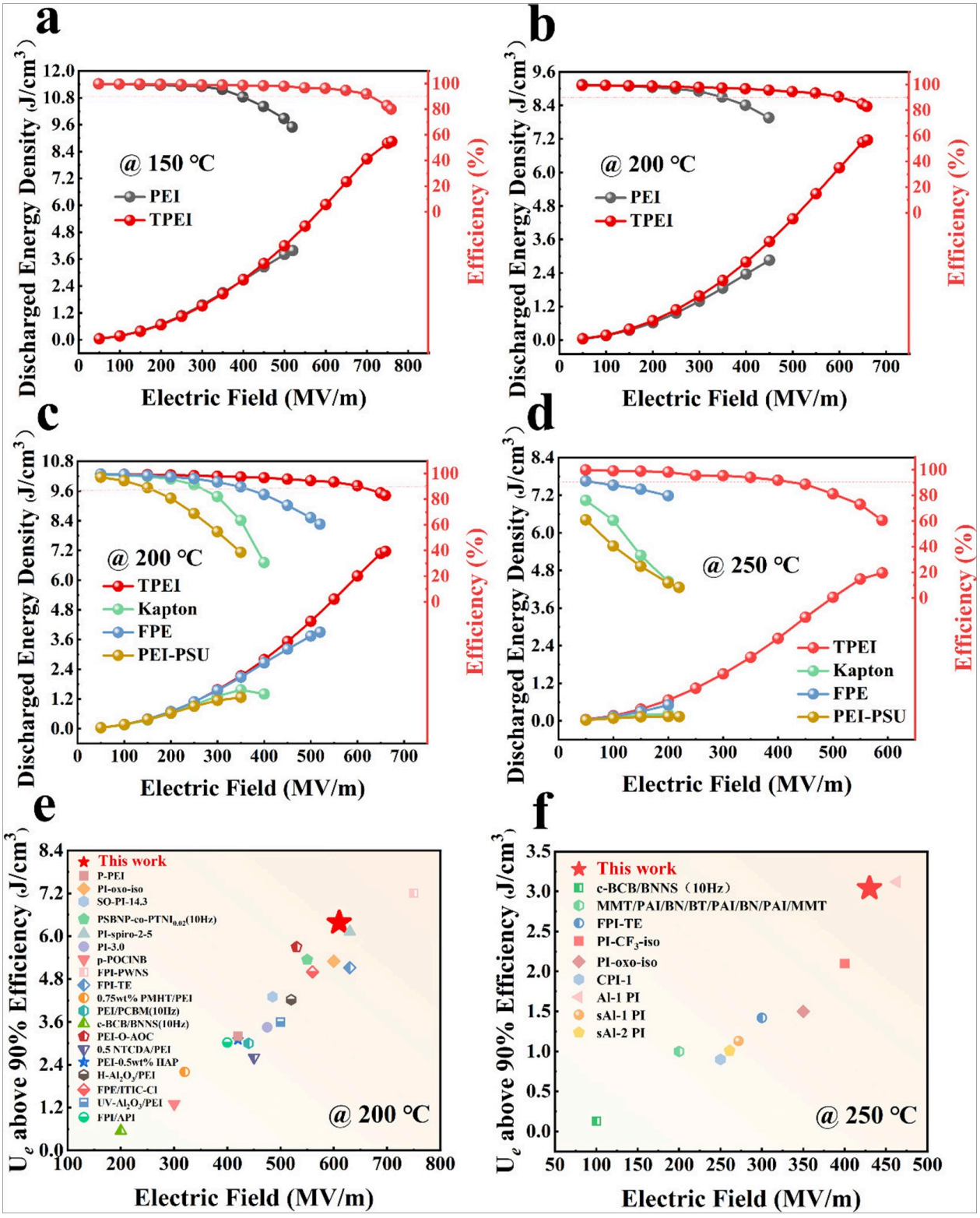

Figure 6

High-temperature insulation properties. Discharge energy density and efficiency versus electric field of PEI and TPEI samples at a) 150 °C and b) 200 °C. Discharge energy density and efficiency versus electric field for TPEI and other polymers (Kapton, FPE, PEI-PSU) at c) 200 °C and d) 250 °C. Comparison of discharge energy density (efficiency > 90%) at e) 200 °C[9, 10, 11, 12, 13, 14, 16, 18, 30, 32, 33, 34, 35, 36, 37, 38, 39, 40, 41] and f) 250 °C[10, 25, 30, 42, 43] for the studied TPEI and the previous work.

Supplementary Files

This is a list of supplementary files associated with this preprint. Click to download.

- supportinginformation.docx